Gold Bull (2014) 47:237–243
DOI 10.1007/s13404-014-0146-9

ORIGINAL PAPER

Phase diagram of Au–Al–Pd at 500 °C

Jyun Lin Li · Pei Jen Lo · Ming Chi Ho · Rick Yu · Ker-Chang Hsieh

Published online: 26 July 2014

Abstract The isothermal phase diagram of Au–Al–Pd at 500 °C was constructed using diffusion couples and equilibrated bulk alloys. Electron microprobe analyses were used to determine the phase compositions and phase relationships. Thirteen three-phase equilibria and two ternary phases (T_1 and T_2) were identified in this study. Phase T_1 contained 37 at% Au, 26 at% Pd, and 37 at% Al. Phase T_2 contained 44 at% Au, 24 at% Pd, and 32 at% Al. The Au solubility in the Al_3Pd_2, AlPd, and $AlPd_2$ phases were 6, 15, and 34 at%, respectively. The Pd solubility in the $AuAl_2$, Au_2Al, Au_8Al_3, and Au_4Al phases were 5, 10, 13, and 3 at%, respectively.

Keywords Phase diagram · Au–Al–Pd · Diffusion couple · Wire bonding

Introduction

Gold wires have been used as bonding wires in integrated circuit (IC) packages because of the ductility and anticorrosion characteristics of gold. Recently, the increase in the input and output (I/O) number of ICs from 200 to 300 has necessitated a decrease in the diameter of gold wires from 25 μm to less than 20 μm to match the decrease in the area of the Al pad. However, the stiffness of gold wires must be enhanced to avoid short circuits caused by wire sweep. Au–Pd alloy wires (such as the Au–1 wt% Pd alloy wire) are one of the several alloy bonding wires that have been recently developed [1]. The bonding wire reacts with the Al pad and forms intermetallic phases to maintain the electrical connection. A low-temperature Au–Al–Pd phase diagram could provide the information required for understanding the reactions between the Au–Pd alloy wire and the Al pad. The stability of the intermetallic phases is closely related to the reliability of wire bonding [1, 2].

In 1991, Okamoto [3] updated the Al–Au phase diagram reported by Murray [4]. In a crystal structure study, the stoichiometry of a compound existing at approximately 72 at% Au was revealed to be in the Au_8Al_3 phase. In accordance with the aforementioned references, the Al–Au phase diagram was revised again by Okamoto in 2005 [5].

The Al–Pd phase diagram was constructed in 1986 by McAlister [6] and revised by Okamoto [7].

Based on the thermodynamic model, Okamoto [8] derived the Au–Pd phase diagram. Three ordered structure phases exist in this system. The Au_3Pd [9] and $AuPd_3$ [10] phases were confirmed by conducting experiments, and the AuPd phase was not confirmed because of its existence at a low temperature (below 100 °C).

In general, isothermal phase diagrams are constructed using bulk alloys, prepared at various compositions, and annealed at a certain high temperature to reach phase equilibrium. Because bulk alloys lead to large dendrites, they require additional time to reach phase equilibrium. According to the references, these bulk alloys require annealing for 14 days at 800 °C [11] and for 30 days at 600 °C [12]. Moreover, depending on the complexity of the isothermal phase diagram, 30 to 50 samples would be required for a study. Because the recovery of Au, a precious metal, is not possible, and a long period is required for the bulk alloys to reach phase equilibrium at low temperatures, this method is too expensive to be used in the present study.

This study focused on the investigation of the Au–Al–Pd phase diagram at 500 °C by combining the diffusion couple technique and the method of equilibrated bulk alloys. The diffusion couple technique follows the principle that phase interface would form local equilibrium, and then, we judge

J. L. Li · P. J. Lo · M. C. Ho · R. Yu · K.-C. Hsieh (✉)
Department of Materials and Optoelectronic Science, National Sun Yat-Sen University, 70, Lien-Hai Road, Kaohsiung 804, Taiwan
e-mail: khsieh@mail.nsysu.edu.tw

Table 1 Summary of phase equilibria in eight diffusion couples

Diffusion couple	Compositions (at%) Al/Au_xPd_{100-x}		Equilibrium phase layers									
	Au	Pd										
D1	90	10	Al	$AuAl_2$	AuAl	Au_2Al	Au_2Al+AlPd	T_1+Au_2Al	T_2	Au_8Al_3+$AlPd_2$	$AlPd_2$+α	α
D2	80	20	Al	$AuAl_2$	AuAl	Au_2Al	Au_2Al+AlPd	T_1	T_2	$AlPd_2$	$AlPd_2$+α	α
D3	70	30	Al	$AuAl_2$	AuAl	Au_2Al	Au_2Al+AlPd	$AlPd_2$	$AlPd_2$+α	α		
D4	60	40	Al	$AuAl_2$	AuAl	Au_2Al	AlPd	$AlPd_2$	$AlPd_2$+α	α		
D5	50	50	Al	Al_4Pd	$Al_{21}Pd_8$	$AuAl_2$+$Al_{21}Pd_8$	$AuAl_2$	$AuAl_2$+AuAl	AlPd	$AlPd_2$	$AlPd_2$+α	α
D6	40	60	Al	Al_4Pd	$AuAl_2$+Al_4Pd	$AuAl_2$+$Al_{21}Pd_8$	$AuAl_2$+Al_3Pd_2	AlPd	$AlPd_2$	α		
D7	30	70	Al	crack	$Al_{21}Pd_8$	$AuAl_2$+$Al_{21}Pd_8$	$AuAl_2$+Al_3Pd_2	AlPd	$AlPd_2$	α		
D8	20	80	Al	Al_4Pd	$AuAl_2$+Al_4Pd	$AuAl_2$+$Al_{21}Pd_8$	$AuAl_2$+Al_3Pd_2	AlPd	phase too small	α		

Table 2 Summary of phase equilibria in seven bulk alloy samples

Alloy	Alloy compositions (at%) ($Au_xPd_yAl_{100-x-y}$)			Phase equilibrium
	Au	Pd	Al	
A1	52	20	28	T_2–Au_8Al_3–$AlPd_2$
A2	48	24	28	Au_8Al_3–$AlPd_2$–α
A3	77	4	19	Au_4Al–Au_8Al_3–α
A4	42	14	44	Au_2Al–AuAl–AlPd
A5	26	52	22	$AlPd_2$–α
A6	68	5	27	Au_4Al–Au_8Al_3
A7	65	30	5	Au_8Al_3–Au_2Al

these phases existing in each other when at the same temperature. This study also referenced the theoretical details of the research conducted by Kodentsov et al. [13].

Experimental procedures

The Au_xPd_{100-x} (x=10 to 80) and $Au_xPd_yAl_{100-x-y}$ alloys were prepared by mini-arc melting pure Au, Pd, and Al in a pure Ar atmosphere. The Au–Pd alloys were arc-melt under Ar atmosphere and turned upside down for seven times and then sucked into 2-mm-diameter copper mold. The ingot length is between 15 and 20 mm. Au–Pd alloy forms a solid solution, and the homogeneity was checked under the electron probe microanalyzer (EPMA). Eight Au–Pd binary alloys (D1–D8) and seven Au–Al–Pd ternary alloys (A1–A7) were prepared for this phase diagram study. The alloy compositions are listed in Tables 1 and 2.

Figure 1 is the schematic diagram of the diffusion couple setup. The Au–Pd binary alloy ingots (D1–D8) were sliced into 1-mm-thick discs, and a pure aluminum bar with a 2-mm diameter was sliced into 2-mm-thick discs. The discs were joined to form a diffusion couple. The screw of the holder exerted pressure on the diffusion couple. The holder was

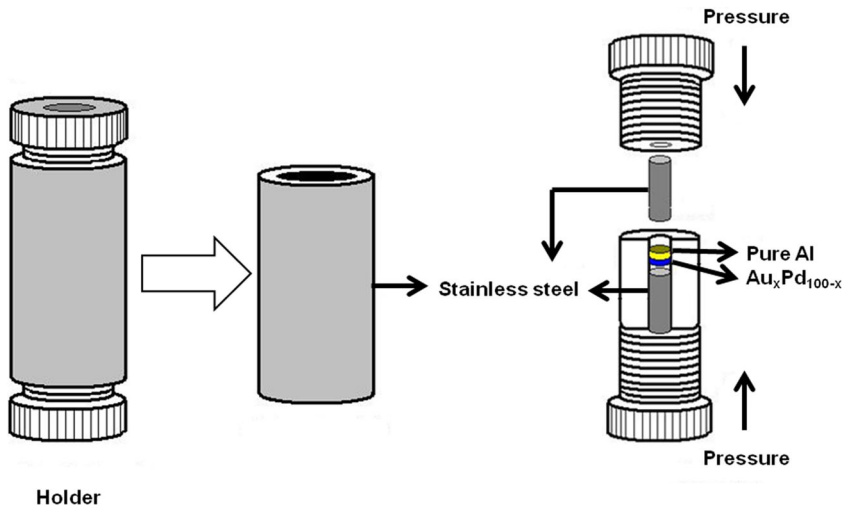

Fig. 1 The sketch diagram of diffusion couple setup

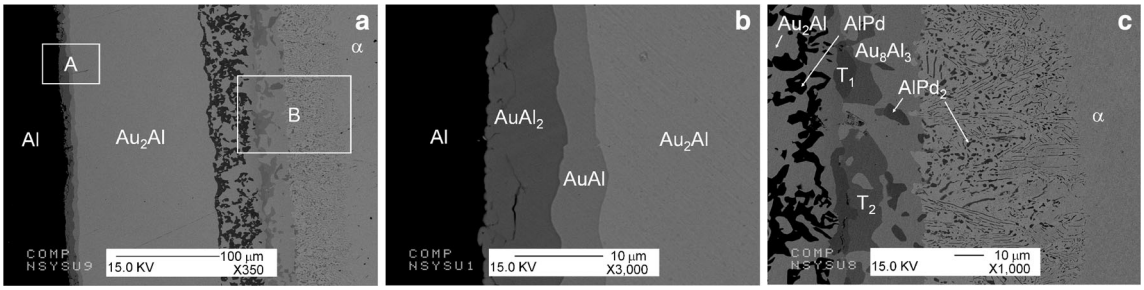

Fig. 2 **a** The whole view of D1 sample microstructure. **b** The detail phase layers of the A region in **a. c** The detail phase layers of the B region in **a**

sealed in a quartz tube in which a vacuum was created and maintained at 500 °C for 24 h; the quartz tube was then quenched in ice water. The ternary alloys (A1–A7) were sealed in the quartz tube vacuum. These alloy samples were maintained at 500 °C for 34 days.

An electron probe microanalyzer (EPMA) was used to determine the equilibrium phase compositions of the diffusion couple samples and ternary alloy samples. The isothermal phase diagram of the Au–Al–Pd alloy annealed at 500 °C was constructed based on these results.

Results

Isothermal section at 500 °C

The phase equilibria of the diffusion couples are summarized in Table 1. As shown in Fig. 2a–c, the D1 diffusion couple formed the equilibrium phase layers $Al/AuAl_2/AuAl/Au_2Al/Au_2Al+AlPd/T_1+Au_2Al/T_2/Au_8Al_3+AlPd_2/AlPd_2+\alpha(Au,Pd)/\alpha(Au,Pd)$. The phase layer thickness of $AuAl_2$, AuAl, and Au_2Al was approximately 10, 5, and 130 μm, respectively, and the Pd solubility was approximately 10 at% in the Au_2Al phase. The T_2–Au_8Al_3–$AlPd_2$ three-phase equilibrium was generated on the interface between the T_2 one-phase layer and $Au_8Al_3+AlPd_2$ two-phase layer. These three-phase equilibria T_2-Au_8Al_3-$AlPd_2$ were confirmed through the bulk alloy (A1) as shown in Fig. 3. The interface between the $Au_8Al_3+AlPd_2$ and $AlPd_2+\alpha$ two-phase layers was also examined. The existence of Au_8Al_3–$AlPd_2$–α three-phase equilibrium was confirmed by analyzing the bulk alloy (A2), as shown in Fig. 4. Four three-phase equilibria were observed in the D1 diffusion layers: Au_2Al–AlPd–T_1, T_1–Au_2Al–T_2, $AlPd_2$–T_2–Au_8Al_3, and α–Au_8Al_3–$AlPd_2$. The phase equilibria of the alloy equilibrium samples are summarized in Table 2. The phase diagram constructed according to the results in Tables 1 and 2 is shown in Fig. 5. In the diffusion-couple experiment, 11 three-phase equilibria, resembling the T_2–Au_8Al_3–$AlPd_2$ or Au_8Al_3–$AlPd_2$–α three-phase equilibria, were determined from the phase relationships. The remaining three-phase equilibria, Au_4Al–α–Au_8Al_3 and Au_2Al–AuAl–AlPd, were determined by applying alloy equilibrium methods to the alloy samples A3 and A4 (Table 2). These 13 sets of three-phase equilibria are shown as solid lines in Fig. 5. In addition, the $AlPd_2$–T_2–AlPd three-phase equilibria were estimated to meet the phase relationships shown as dashed

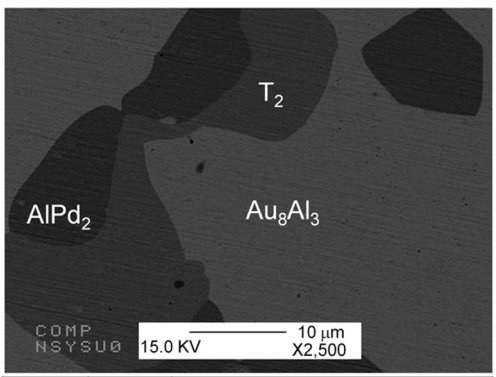

Color	Phase	Composition (at.%)		
		Pd	Au	Al
light gray	Au_8Al_3	12.34±0.39	61.48±0.49	26.18±0.54
dark gray	T_2	24.42±0.19	43.93±0.30	31.65±0.22
black	$AlPd_2$	33.16±0.27	33.91±0.50	32.94±0.41

Fig. 3 The microstructure of A1 alloy sample including Au_8Al_3, T_2 and $AlPd_2$ phases

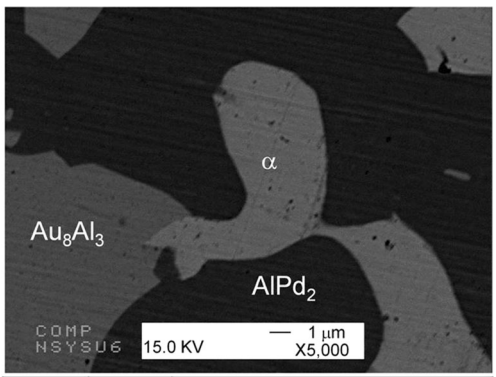

Color	Phase	Composition (at.%)		
		Pd	Au	Al
light gray	α	4.68±0.11	83.06±0.17	12.26±0.13
dark gray	Au_8Al_3	13.26±0.39	60.43±0.42	26.31±0.15
black	$AlPd_2$	34.49±0.14	32.60±0.49	32.91±0.35

Fig. 4 The microstructure of A2 alloy sample including Au_8Al_3, α(Au,Pd) and $AlPd_2$ phases

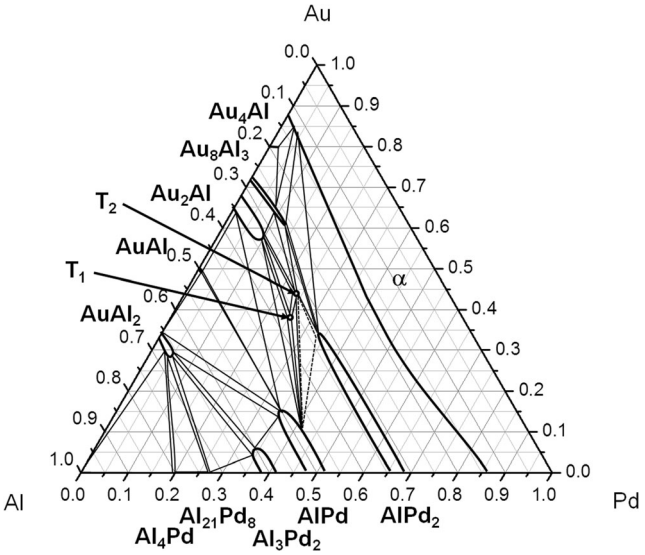

Fig. 5 The isotherm of Au-Al-Pd at 500 °C determined by this study

lines in Fig. 5. This experiment revealed that most binary phases conform to the Al–Au [5] and Al–Pd [7] binary phase diagrams. The Au–Pd [8] system exists in the α phase only at 500 °C. In this study, Al solubility in the α phase was also determined. In the experiment, 13 three-phase equilibria were observed in the Au–Al–Pd ternary system: T_2–Au_2Al–Au_8Al_3, T_1–Au_2Al–T_2, T_1–Au_2Al–AlPd, AuAl–AlPd–Au_2Al, $AuAl_2$–AlPd–AuAl, $Al_{21}Pd_8$–$AuAl_2$–Al_3Pd_2, AlPd–$AuAl_2$–Al_3Pd_2, Al_4Pd–$AuAl_2$–$Al_{21}Pd_8$, Al–$AuAl_2$–Al_4Pd, T_1–AlPd–T_2, T_2–$AlPd_2$–Au_8Al_3, $AlPd_2$–Au_8Al_3–α, and Au_4Al–Au_8Al_3–α. The three-phase equilibrium AlPd–T_2–$AlPd_2$ was estimated to demonstrate the phase relationship. T_1 and T_2 are newly discovered ternary phases.

Solubility range of binary intermetallic phases

The Au solubility in the Al_3Pd_2, AlPd, and $AlPd_2$ phases was 6, 15, and 34, respectively. The Pd solubility in $AuAl_2$, Au_2Al, and Au_8Al_3 phases was 5, 10, and 13 at%, respectively. In the Au_4Al phase, Al atoms were exchanged with Pd atoms, and the Pd solubility in the Au_4Al phase was 3 at%. The maximal solubility of the $AlPd_2$ and Au_8Al_3 phases was determined based on the bulk alloys (A2) shown in Fig. 4. The Al_4Pd, $Al_{21}Pd_8$, and AuAl phases exhibited extremely low solubility.

T_1 and T_2 ternary phases

The T_1 and T_2 phases were observed in the D1 and D2 diffusion couple. The compositions of the T_1 and T_2 ternary phases were determined by conducting EPMA analysis on the D1 and D2 diffusion samples, as shown in Fig. 6. The T_1 phase contained 37 at% Au, 26 at% Pd, and 37 at% Al. The T_2 phase contained 44 at% Au, 24 at% Pd, and 32 at% Al.

Discussion

In this study, a classical semiinfinite diffusion couple was applied, meaning that the end couples maintained their original compositions after the diffusion couple was annealed. If volume diffusion in a semiinfinite couple is observed to be a rate-limiting step, a local equilibrium is assumed to exist; therefore, the rules described previously can be applied to relate the reaction zone morphology developed during isothermal diffusion to the phase diagram. The phase composition of the reaction zone is independent of time, whereas that of the diffusion path is fixed. The effectiveness of this technique in constructing isothermal cross-sections of ternary systems has been documented extensively [13].

The bulk alloy compositions and D2 and D6 diffusion paths are marked in Fig. 7. The microstructure of the D2 diffusion couple is shown in Fig. 8a, b. The D2 diffusion couple formed the equilibrium phase layers Al/$AuAl_2$/AuAl/Au_2Al/Au_2Al+AlPd/T_1/T_2/$AlPd_2$/$AlPd_2$+α(Au,Pd)/α(Au,Pd). A two-phase layer (Au_2Al+AlPd) was in contact with the T_1 phase layer; therefore, the Au_2Al–AlPd–T_1 three-phase equilibrium was generated. The D2 diffusion path is plotted in Fig. 8c, and its corresponding microstructure is shown in Fig. 8a, b. The solid a–b line crosses the α(Au, Pd) single-phase field, b–c is in the $AlPd_2$-α(Au, Pd) two-

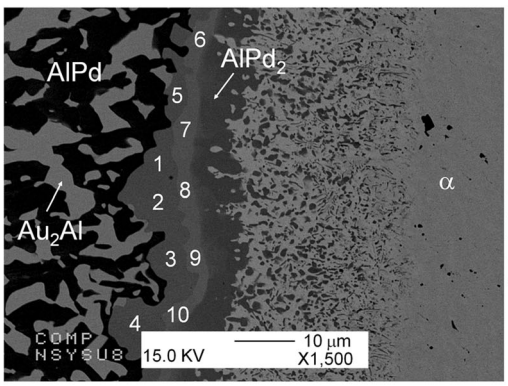

No.	Phase	Composition (at.%)		
		Pd	Au	Al
1	T_1	26.76	36.89	36.36
2	T_1	26.52	36.96	36.52
3	T_1	26.81	36.04	37.14
4	T_1	25.57	37.22	37.21
5	T_1	25.96	37.22	36.82
6	T_2	24.82	43.16	32.02
7	T_2	24.75	43.07	32.18
8	T_2	24.79	42.40	32.81
9	T_2	25.38	41.83	32.78
10	T_2	25.52	41.25	33.22

Phase	Composition (at.%)		
	Pd	Au	Al
T_1	26.32±0.48	36.87±0.43	36.81±0.34
T_2	25.05±0.33	42.34±0.73	32.6±0.44

Fig. 6 The compositions of T_1 and T_2 ternary phases determined from D2 diffusion couple sample

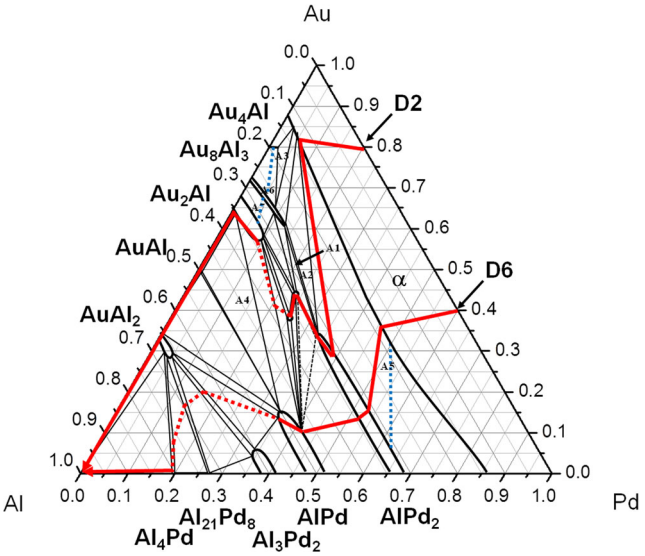

Fig. 7 The bulk alloy samples and the diffusion paths of D2 and D6 samples

phase region, c–d is in the $AlPd_2$ phase region, e–f is in the T_2 phase region, g–h is in the T_1 phase region, and the dashed h–i line crosses the Au_2Al–AlPd–T_1 three-phase region, indicating the presence of an interface in the diffusion couple, with equilibrium between the single-phase T_1 and Au_2Al–AlPd two-phase region. The j–k–l–m–n–o–p line in Fig. 8c shows that the diffusion path crosses four single-phase layers, the Au_2Al, AuAl, and $AuAl_2$ phases and the Al end phase. The phase layer thickness of $AuAl_2$, AuAl, and Au_2Al was approximately 24, 35, and 50 μm, respectively. There are voids formed within the phase layer such as AuAl phase in Fig. 8a or Kirkendall voids build up at interface. If the diffusion couples were held for longer time, crack may form between certain phase layers.

The D6 diffusion path crossed three three-phase regions ($AuAl_2$–AlPd–Al_3Pd_2, $AuAl_2$–Al_3Pd_2–$Al_{21}Pd_8$, and $AuAl_2$–$Al_{21}Pd_8$–Al_4Pd) with $AuAl_2$ as the common matrix phase. Figure 9a shows the diffusion path near the Al–Pd binary region, and Fig. 9b shows the plot displaying the equilibrium of these three phases and their related two-phase regions. According to Fig. 9b, f–g is the $AuAl_2$–AlPd–Al_3Pd_2 three-phase equilibrium, g–h is the $AuAl_2$–Al_3Pd_2 two-phase region, h–i is the $AuAl_2$–Al_3Pd_2–$Al_{21}Pd_8$ three-phase equilibrium, i–j is the $AuAl_2$–$Al_{21}Pd_8$ two-phase region, j–k is the $AuAl_2$–$Al_{21}Pd_8$–Al_4Pd three-phase equilibrium, k–l is the $AuAl_2$–Al_4Pd two-phase region, and l–m is the Al_4Pd single-phase region, and then in equilibrium with the Al edge phase. The microstructure and corresponding sketch are shown in Fig. 9c and are labeled from f to m, as described previously.

For the wire bonding process, Fig. 10 shows the microstructure of the Au–0.9Pd wire sample under 165 °C and 3,000-h aging [1]. The $(Au, Pd)_4Al$ and Au_5Al_2 (as Au_8Al_3) phases tangled with the Pd-rich layer as α(Au, Pd). Because these three phases will maintain three-phase equilibrium as this study and this stable interface can hold for long time means better wire bond reliability.

For the intermetallic phases, $AuAl_2$ is purple and used for jewellery applications. The solubility of Pd in the purple $AuAl_2$ phase is limited in Fig. 8a and has 5 at% in D5

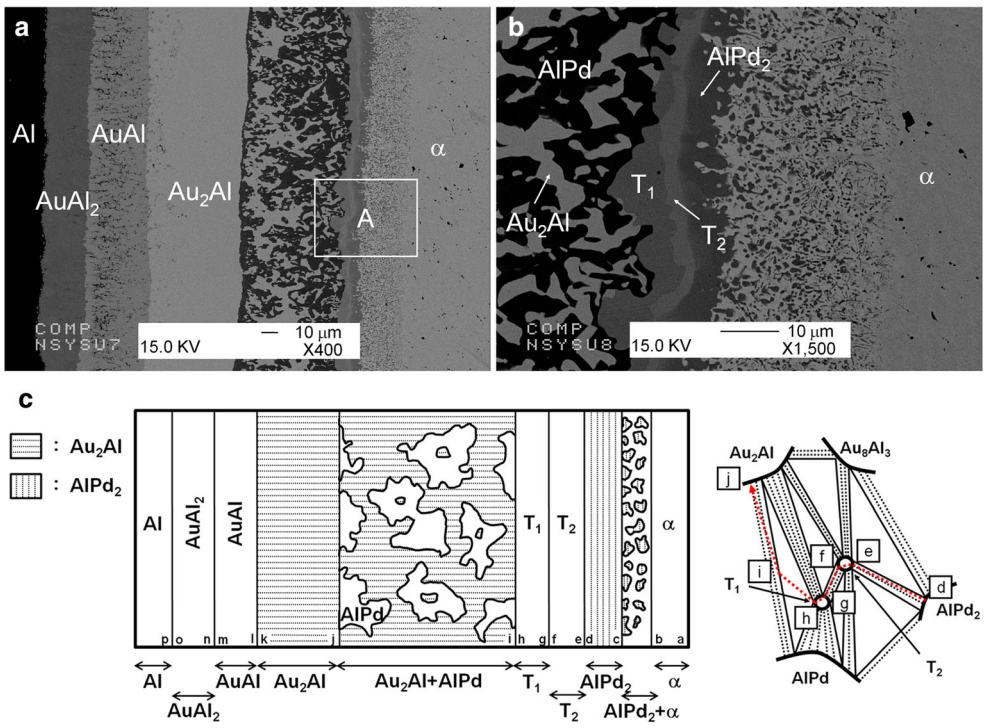

Fig. 8 **a** The whole view of D2 sample microstructure. **b** The detail phase layers of the A region in **a. c** The diffusion path of D2 diffusion couple and sketch figure

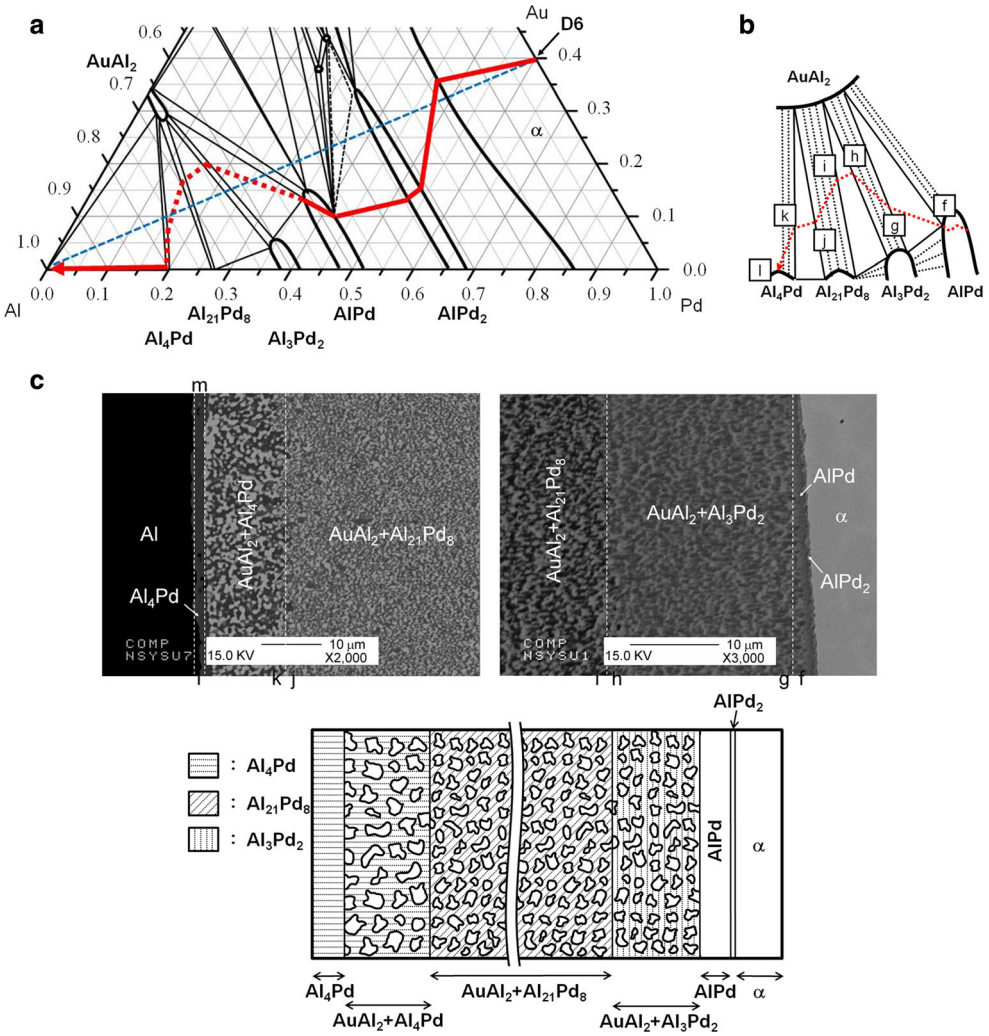

Fig. 9 **a** The diffusion path of D6 diffusion couple near the Al–Pd binary region. **b** The sketch figure of D6 diffusion path. **c** The microstructure of D6 diffusion couple with the label (f to m) and sketch figure

diffusion couple. And both $AuAl_2$ phase still maintain purple color.

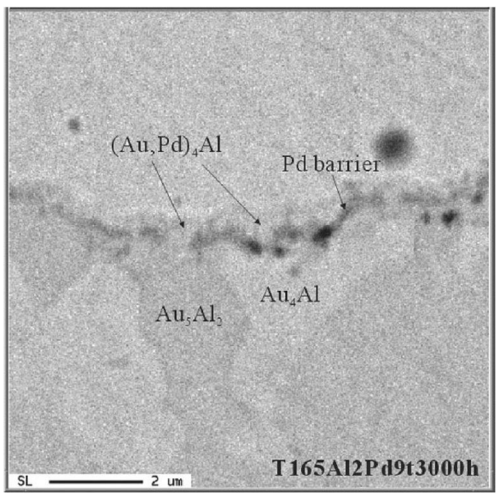

Fig. 10 The microstructure of the Au–0.9Pd wire sample under 165 °C and 3,000-h aging [1]

Conclusion

This study is the first to investigate a Au–Al–Pd system. The isothermal section of a Au–Al–Pd system annealed at 500 °C was presented in this study. The entire composition range included two ternary phases (T_1 and T_2) and 14 three-phase equilibria: T_2–Au_2Al–Au_8Al_3, T_1–Au_2Al–T_2, T_1–Au_2Al–AlPd, AuAl–AlPd–Au_2Al, $AuAl_2$–AlPd–AuAl, $Al_{21}Pd_8$–$AuAl_2$–Al_3Pd_2, AlPd–$AuAl_2$–Al_3Pd_2, Al_4Pd–$AuAl_2$–$Al_{21}Pd_8$, Al–$AuAl_2$–Al_4Pd, T_1–AlPd–T_2, T_2–$AlPd_2$–Au_8Al_3, $AlPd_2$–Au_8Al_3–α, and Au_4Al–Au_8Al_3–α. The three-phase equilibrium AlPd–T_2–$AlPd_2$ was estimated to exhibit the phase relationship. T_1 and T_2 are newly discovered ternary phases. The T_1 phase contained 37 at% Au, 26 at% Pd, and 37 at% Al. The T_2 phase contained 44 at% Au, 24 at% Pd, and 32 at% Al.

The Au solubility in the Al_3Pd_2, AlPd, and $AlPd_2$ phases was 6, 15, and 34 at%, respectively, by exchanging Pd atoms. The Pd solubility in the $AuAl_2$, Au_2Al, and Au_8Al_3 phases was 5, 10, and 13 at%, respectively, by exchanging Au atoms.

The Pd solubility in Au_4Al phase was 3 at% by exchanging Al atoms.

Acknowledgments We acknowledge the financial support provided by the National Science Council, Grant No. NSC 98-2221-E-110-034-MY3, for this research.

References

1. Chang HS, Hsieh KC, Martens T, Yang A (2003) The effect of Pd and Cu in the intermetallic growth of alloy Au wire. J Electron Mater 32: 1182–1187
2. Gam SA, Kim HJ, Cho JS, Park YJ, Moon JT, Paik KW (2006) Effects of Cu and Pd addition on Au bonding wire/Al pad interfacial reactions and bond reliability. J Electron Mater 35:2048–2055
3. Okamoto H (1991) Al-Au (Aluminum-Gold). J Phase Equilib 12: 114–115
4. Murray JL, Okamoto H, Massalski TB (1987) The Al-Au (Aluminum-Gold) system. Bull Alloy Phase Diagr 8:20–29
5. Okamoto H (2005) Al-Au (Aluminum-Gold). J Phase Equilib Diffus 26:391–393
6. McAlister AJ (1986) The Al-Pd (Aluminum-Palladium) system. Bull Alloy Phase Diagr 7:368–374
7. Okamoto H (2008) Al-Pd (Aluminum-Palladium). J Phase Equilib Diffus 29:199
8. Okamoto H, Massalski TB (1985) The Au-Pd (Gold-Palladium) system. Bull Alloy Phase Diagr 6:229–235
9. Nagasawa A, Matsuo Y, Kakinoki J (1965) Ordered alloys of gold-palladium system. I. Electron diffraction study of evaporated Au_3Pd films. J Phys Soc Jpn 20:1881–1885
10. Matsuo Y, Nagasawa A, Kakinoki J (1966) Ordered alloys of the gold-palladium system. II. Electron diffraction study on evaporated $AuPd_3$ films. J Phys Soc Jpn 21:2633–2637
11. Liu CH, Chiang WR, Hsieh KC, Austin Chang Y (2006) Phase equilibrium in the Cu-Ni-Zr system at 800 °C. Intermetallics 14: 1011–1013
12. Seropegin YD, Gribanov AV, Kubarev OL, Tursinaa AI, Bodakb OI (2001) Isothermal cross-section of the Ce-Pd-Si phase diagram at 600 °C. J Alloys Compd 317:320–323
13. Kodentsov AA, Bastin GF, Van Loo FJJ (2001) The diffusion couple technique in phase diagram determination. J Alloys Compd 320:207–217